Published in final edited form as:
Opt Express. 2010 September 13; 18(19): 20029–20048.

Ultrahigh speed 1050nm swept source / Fourier domain OCT retinal and anterior segment imaging at 100,000 to 400,000 axial scans per second

Benjamin Potsaid[1,2], **Bernhard Baumann**[1,3], **David Huang**[4], **Scott Barry**[2], **Alex E. Cable**[2], **Joel S. Schuman**[5], **Jay S. Duker**[3], and **James G. Fujimoto**[1,3,*]

[1] Department of Electrical Engineering and Computer Science, and Research Laboratory of Electronics, Massachusetts Institute of Technology, Cambridge, MA 02139, USA

[2] Advanced Imaging Group, Thorlabs, Inc., Newton, NJ 07860, USA

[3] New England Eye Center and Tufts Medical Center, Tufts University, Boston, MA 02116, USA

[4] Doheny Eye Institute, University of Southern California, Los Angeles, CA 90033, USA

[5] UPMC Eye Center, University of Pittsburgh, Pittsburgh, PA 15213, USA

Abstract

We demonstrate ultrahigh speed swept source/Fourier domain ophthalmic OCT imaging using a short cavity swept laser at 100,000–400,000 axial scan rates. Several design configurations illustrate tradeoffs in imaging speed, sensitivity, axial resolution, and imaging depth. Variable rate A/D optical clocking is used to acquire linear-in-k OCT fringe data at 100kHz axial scan rate with 5.3um axial resolution in tissue. Fixed rate sampling at 1 GSPS achieves a 7.5mm imaging range in tissue with 6.0um axial resolution at 100kHz axial scan rate. A 200kHz axial scan rate with 5.3um axial resolution over 4mm imaging range is achieved by buffering the laser sweep. Dual spot OCT using two parallel interferometers achieves 400kHz axial scan rate, almost 2X faster than previous 1050nm ophthalmic results and 20X faster than current commercial instruments. Superior sensitivity roll-off performance is shown. Imaging is demonstrated in the human retina and anterior segment. Wide field 12×12mm data sets include the macula and optic nerve head. Small area, high density imaging shows individual cone photoreceptors. The 7.5mm imaging range configuration can show the cornea, iris, and anterior lens in a single image. These improvements in imaging speed and depth range provide important advantages for ophthalmic imaging. The ability to rapidly acquire 3D-OCT data over a wide field of view promises to simplify examination protocols. The ability to image fine structures can provide detailed information on focal pathologies. The large imaging range and improved image penetration at 1050nm wavelengths promises to improve performance for instrumentation which images both the retina and anterior eye. These advantages suggest that swept source OCT at 1050nm wavelengths will play an important role in future ophthalmic instrumentation.

1. Introduction

Optical coherence tomography (OCT) interferometrically detects backscattered light to perform micron level two and three dimensional imaging of tissue with high sensitivity and dynamic range [1]. In ophthalmology, OCT is widely used for non-invasive structural and

*jgfuji@mit.edu.

quantitative imaging of the retina and anterior segment. OCT enables identification of pathologies for disease diagnosis and monitoring response to therapy [2].

Early OCT systems used low coherence interferometry with a mechanically swept reference mirror to measure the echo delay of backscattered light (time domain OCT). Commercial ophthalmic OCT instruments operated at speeds of 100–400 axial scans per second. A limited number of cross sectional images could be acquired because blinking and eye motion limited data acquisition times. A different detection scheme, Fourier domain OCT, can be implemented using a broadband light source, spectrometer and line scan camera (spectral domain OCT) or using a wavelength swept laser, single or dual balanced detector and high speed A/D (swept source OCT) [3]. Fourier domain detection has a fundamental sensitivity advantage which enables orders of magnitude faster imaging speeds compared to time domain OCT [4–6].

The first demonstration of spectral/Fourier domain OCT for *in vivo* retinal imaging was performed in 2002 [7]. Ultrahigh axial resolutions of 2.1 to 3.5μm in the retina at ~10kHz to ~29kHz axial scan rates were demonstrated in 2004 [8–10]. In 2006, the first commercial ophthalmic OCT instruments using spectral/Fourier domain OCT were introduced. Spectral/Fourier domain OCT instruments measure interference spectra using a spectrometer and line scan camera. The limited number of camera pixels results in a design trade-off between OCT axial resolution and imaging range. Current commercial ophthalmic OCT instruments typically achieve ~5μm axial resolution with ~25–27kHz axial scan rates over an imaging range of ~2.0–2.6mm. Instruments such as the Optopol Copernicus HR operate with 3μm axial resolution at 52kHz. Other instruments, such as the Heidelberg Spectralis, have axial resolution of 7μm at 40kHz. In these systems, performance tradeoffs in imaging speed, imaging range, and axial resolution have been governed by commercially available CCD linescan camera technology. Recently, research OCT instruments using high speed CMOS cameras have been demonstrated for retinal imaging at record 312kHz axial scan rates [11]. However, operating at high imaging speeds requires short camera exposure times, resulting in reduced sensitivity. Although good quality images can be obtained in young subjects and normal eyes at imaging speeds from 70 to 312kHz axial scan rates with 850nm wavelengths [11], the practicality of imaging at speeds much greater than ~100kHz with such technology in the clinic is not clear because many patients have cataracts and ocular opacities, which reduce signal strength and image quality.

Swept source/Fourier domain OCT [3] offers several advantages over spectral/Fourier domain OCT, including reduced fringe washout, better sensitivity with imaging depth (lower sensitivity roll-off), longer imaging range, higher detection efficiencies (because there are no spectrometer grating losses), and ability to perform dual balanced detection. Early wavelength swept laser sources using a variety of laser tuning mechanisms, including rotating polygon mirrors [12] and galvo driven grating filters [13], achieved axial scan speeds in the ~10–50kHz range at wavelengths of ~1050nm [12, 14] and ~850nm [13, 15, 16] for retinal imaging. The long length of these laser cavities limited the maximum laser sweep rates because of the time required for a sufficient number of laser round trips through the gain medium and filter to achieve saturation and suppression of ASE noise (amplified spontaneous emission) from the laser gain element [17]. The introduction of Fourier domain mode locking (FDML) enabled dramatic increases in sweep speeds by using a long fiber optic delay line in the laser cavity to store the entire frequency sweep while synchronously tuning the intracavity filter with the sweep [18]. Recently, by combining a fast laser sweep repetition rate with multiple spot imaging, an FDML laser operating at 1310nm was used to generate 3D-OCT volumes at record imaging rates of 20.8 Million axial scans per second with 13μm axial resolution and record data acquisition rates of 4.5 GVoxel per second with 11μm axial resolution in tissue [19]. Retinal imaging cannot be performed at 1310nm

because of water absorption. Ultrahigh speed swept source OCT retinal imaging using an FDML laser operating at 1060nm with an axial scan rate of 249kHz and an 8μm axial resolution in tissue [20] has been demonstrated. Anterior segment imaging at 200kHz with 9μm axial resolution over a 2mm imaging range and 25μm axial resolution over an 8mm imaging range using an FDML laser at 1310nm has also recently been performed [21].

Increased penetration into the choroid and optic nerve head with reduced sensitivity to ocular opacities has been demonstrated for OCT imaging in the water absorption window at ~1050nm [14, 22, 23] compared to 850nm wavelengths. Imaging at 1050nm can be performed with spectral/Fourier domain OCT using InGaAs linescan cameras or with swept source/Fourier domain OCT using swept lasers. The width of the 1050nm water absorption window limits the achievable axial resolution [24]. Imaging at 850nm permits higher axial resolution and appears to provide higher inner retinal layer contrast than 1050nm [25]. Although the clinical utility of 1050nm OCT imaging is yet to be determined, recent research results from prototype systems suggest 1050nm imaging may become an important clinical technology for ophthalmology due to enhanced imaging range and penetration through tissue and ocular opacities [26, 27].

In this paper, we demonstrate ultrahigh speed swept source/Fourier domain ophthalmic OCT imaging at speeds of 100,000–400,000 axial scan rates using a new commercially available swept laser centered at ~1050nm. Four imaging configurations are characterized and demonstrated for retinal and anterior segment imaging. A first configuration images at 100kHz axial scan rate with 5.3μm axial resolution in tissue and uses an optically derived, variable frequency clock for the high speed A/D acquisition. This optical clocking method samples the nonlinearly swept waveform at equal wavenumber (k) intervals, thereby eliminating the need to perform numerical k calibration and sweep linearization. Sweep-to-sweep variation is accommodated in real time with this method. Two dimensional cross sectional OCT images and dense three dimensional raster scanned volumes of the macula, disc, and anterior segment are demonstrated. A second configuration images at 100kHz axial scan rate with a 1 GSPS A/D sample rate and uses numerical k calibration to linearize the fringe signal to achieve axial resolution of 6.0μm over a long 7.5mm in tissue (10mm in air) imaging range. This configuration is used to image the anterior segment, enabling visualization of the cornea, iris, and anterior lens in a single image. A third configuration images at 200kHz axial scan rate by buffering and multiplexing the laser sweep using a long optical fiber. A fixed A/D sampling rate of 400 MSPS with numerical k calibration enables an extended imaging range over the optically clocked configuration. The high imaging speeds of this configuration are used to demonstrate wide field 12mmx12mm (1100×1100 axial scan) OCT volumetric raster scans that include the optic nerve head and macula in a single acquisition. Individual cone photoreceptors can be visualized in certain regions of the retina when zooming in to image small, high sampling density 700μm×700μm volumes at 200kHz axial scan rate. Multiple small volumes were acquired and show increasing photoreceptor spacing from the fovea to optic nerve head. A fourth configuration achieves 400kHz axial scan rates by projecting two spots on the retina and detecting with two parallel interferometers. To the best of our knowledge, 400kHz axial scan rate is the fastest speed demonstrated for imaging the retina. The 400kHz axial scan rate is almost twice as fast as previously reported for 1050nm retinal imaging [20] and twenty times faster than most current commercial OCT instruments. As demonstrated in this paper, multi-spot retinal imaging may be an enabling approach for obtaining wide field, large volume acquisitions within the short 2–3 second imaging times required for clinical ophthalmic imaging.

In all configurations, the long coherence length of the swept laser shows significantly improved imaging depth range and less sensitivity roll-off with depth when compared to spectral/Fourier domain OCT. It is common when imaging patients in a clinical setting that

the eye move in the axial direction relative to the instrument due to heartbeat and breathing, as well as gross head movement within the instrument chin rest. The improved sensitivity roll-off performance enables high signal strength images to be obtained over an extended imaging depth range, which promises to improve performance in the clinic where patient head and eye movements in the axial direction can compromise data quality. The improved performance of 1050nm wavelength imaging through cataracts and ocular opacities, improved image penetration into the optic nerve head and choroid, high instrument sensitivity at 100kHz to 400kHz axial scan rates, and long imaging range promise to enable practical ultrahigh speed OCT imaging in the ophthalmology clinic. Furthermore, these results show that a single ultrahigh speed ophthalmic system can image both the retina and anterior eye at 1050nm to achieve a good balance between axial resolution and penetration/imaging range. Results suggest that ophthalmic OCT imaging systems using swept source/Fourier domain OCT detection, new swept laser technology, sweep buffering, and multi-spot imaging may have a powerful impact on clinical ophthalmic imaging, as well as in other applications.

All of the prototype ophthalmic OCT imaging configurations use swept source/Fourier domain detection. The systems are summarized in Table 1 and the layouts of the optical systems are shown in Fig. 1. A commercially available swept laser at ~1050nm (Axsun Technologies, Inc.) with ~100nm full width sweep bandwidth operates at a 100kHz repetition rate, as shown in Figs. 2(A) and 2(B). The laser consists of a semiconductor gain element and high finesse tunable filter with a short cavity length to enable rapid tuning. As shown in Fig. 1(A), the laser is connected to a 50:50 fiber coupler (for output power attenuation) to generate a 100kHz swept laser source. As shown in Fig. 2(B), during the backward sweep, the laser is turned off. The duty cycle of the sweep is only slightly larger than 50 percent, so the effective repetition rate of the laser can be doubled by buffering and multiplexing the sweep, as shown in Fig. 1(B). The laser sweep is split by a 60:40 fiber coupler and the original sweep from the 40 percent output is directed to the 50:50 fiber coupler for multiplexing. A ~1km length of fiber is used to delay the sweep from the 60 percent output by one half of the sweep period such that a “copy” of the sweep can be combined with the original sweep during the time period when the laser is off, as shown in Fig. 2(D). Polarization controls are used to match the polarization states of the two sweeps. This generates a 200kHz repetition rate sweep at the outputs labeled 2 and 3 in Fig. 1(B). Figure 1(C) shows a schematic of the OCT interferometer and patient interface for retinal imaging. Light from output 1, 2, or 3 in Fig. 1(A) or (B) is coupled into a 50:50 (Configuration C) or 70:30 (Configurations A, B, and D) fiber coupler in the interferometer(s). A portion of the light proceeds to the patient interface and the other portion to the reference arm. The average output power of the laser is ~18mW. Retinal exposures were 1.9mW or less, consistent with safe ocular exposure limits set by the American National Standards Institute (ANSI). When imaging at 100kHz and 200kHz, the exposure was 1.8mW. At 400kHz, the exposure in each of the two spots was 950μ W each, totaling 1.9mW. A 70:30 fiber coupler is used for the 100kHz and 400kHz configurations to attenuate the power before reaching the eye and also has the advantage of increasing the amount of light to the interferometer that is collected by the patient interface. The sweep buffering stage introduces considerable power attenuation. When imaging at 200kHz, a 50:50 fiber coupler is used to obtain 1.8mW on the eye. For anterior segment imaging, the patient interface module is modified to telecentrically scan a focused beam, as shown in Fig. 1(D). Light backscattered from the eye is collected by the patient interface module and interferes with the reference arm light at a 50:50 fiber coupler. A balanced detector with InGaAs photodiodes is sampled with a high speed 14 bit 400MHz A/D card (Innovative Integration X5-400M) or 8 bit digital storage scope (Tektronix DPO 7104) set to sample at 1 GSPS to record the interferometric signal. To achieve 400kHz axial scan rates, two separate imaging spots, each with its own interferometer, were projected onto the eye. Output

number 2 in Fig. 1(B) supplies light to the first interferometer and output number 3 in Fig. 2(B) supplies light to the second interferometer. Two separate balanced detectors were used to measure the signals from the two interferometers. Because the laser sweep is nonlinear in time (red lines in Fig. 2(C) show the sweep phase vs. sample number), the sweep must be either optically clocked or calibrated to be linear in k (or frequency). The sweep calibration can be determined experimentally by directing the reference arm light to a Michelson interferometer and detecting the output interference fringe signal with a single (non-balanced) channel of the detector, as shown in Fig. 1(E). The Michelson calibration technique requires manual fiber connections, but has the advantage of being dispersion balanced and time delay matched because the same detector and electrical path are used for calibration and imaging.

A beam diameter of 1.4mm ($1/e^2$ diameter) on the cornea enables a long depth of field (Raleigh range) for long depth range imaging. Changing the eye lens [Fig. 1(C)] to achieve 3.3mm beam diameter improves transverse resolution for imaging small features, however depth of field is reduced. For anterior imaging, the 0.035NA configuration achieves high lateral resolution, while the 0.024NA configuration achieves a long focal length for extended depth imaging. Beam diameters were measured with a beam profiler (DataRay WinCamD).

2.2. Sample clocking and wavelength calibration

Swept source OCT imaging systems typically have a nonlinear frequency sweep in time and require a numerical calibration of the raw fringe data to achieve equal sample spacing in k (or frequency) to linearize the fringe. Mach-Zehnder [18] or Michelson [21] interferometers can be used to generate a calibration trace at a fixed interferometer delay. The calibration can be applied to every laser sweep individually to account for sweep-to-sweep variation [21] caused by dynamic instabilities in the high speed tunable optical filter, however this requires two simultaneous channels of high speed acquisition as well as substantial post processing. One representative calibration can be applied to multiple lines of acquisition [28], however imaging performance can be degraded if the high speed tunable optical filter has mechanical resonances causing sweep-to-sweep variation. Attempts to linearize the sweep profile by optimizing the filter driving waveform trajectory can address sweep nonlinearity, but do not explicitly address sweep-to-sweep variation [29].

By clocking the high speed A/D with a signal derived from an interferometer and conditioned with electronics both integrated in the commercial light source, the fringe can be automatically sampled at intervals with equal k (or frequency) spacing, to produce a linearized fringe signal. This allows a direct Fourier transform of the fringe data to generate OCT intensity images and eliminates the need for the Michelson or Mach-Zehnder calibration and fringe linearization procedure. Furthermore, provided that the optical clock is stable, the data is properly sampled, even with sweep-to-sweep variation. Similar approaches for A/D clocking to achieve uniform k-space sampling have been previously described [30, 31]. These approaches also reduce the data transfer and storage requirements for the raw fringe data because the slower frequency sweep portions of the fringe are not oversampled.

The commercially available short cavity swept laser used in this study provides an A/D clock signal output, which was used to clock the high speed A/D data acquisition board. A start-of-sweep trigger from the laser source was used to trigger the A/D data acquisition through a pulse generator/delay. Figure 2(B) shows the start-of-sweep trigger, laser output, and optically derived clock signal. The clock is synthesized from the laser output, so is only valid during the time when the laser is on. When the laser is off, the swept source generates an asynchronous clock signal, as shown in Fig. 2(B). The optical clock works for the

specific A/D used in these studies, however some A/Ds require continuous clock signals with precise duty cycles, without dropouts or phase discontinuities. For the system used in this study, occasional clock instabilities occurred, resulting in distorted axial scans with loss of resolution and increased background levels. Example fringes acquired using a fixed frequency 400 MSPS sampling rate and the optical clocking scheme for a fringe generated from reflections at two depth positions are shown in Fig. 2(C). The red line indicates fringe phase vs. sample point. Note the nonlinearity in the phase curve for the fixed 400 MSPS data compared to the linearized fringe from the optically clocked data set. Results from a direct Fourier transform of the clock signal indicate a maximum clock frequency of only ~310MHz, which implies that the 400MHz sampling configuration should have a longer imaging range than the optically clocked configuration.

Figure 2(B) shows that the optically derived clock is only valid during the laser sweep. When buffering the laser to achieve a 200kHz repetition rate, the A/D is operated at a constant 400 MSPS sampling rate using an internal clock and software fringe linearization is performed. The reference trace for the software calibration is obtained from a Michelson interferometer, as shown in Fig. 1(E), which has the advantage of being dispersion balanced to separate the effects of sweep nonlinearity from dispersion mismatch. A similar software fringe linearization approach was used for the 100kHz axial scan rate configuration with digital storage scope acquisition set to sample at 1 GSPS and the 400kHz axial scan rate dual beam configuration.

2.3. Computer, data acquisition, electronics and control

Ultrahigh speed OCT can acquire large data sets within only a few seconds acquisition time. To allow data sets greater than the 4 Gigabytes supported by 32 bit operating systems, the instrument control computer used a 64 bit operating system (Windows Vista 64). The high speed A/D card can sample up to 400 MSPS at 14 bit resolution. Data acquisition at 100kHz to 200kHz is performed using one A/D card in the computer. However, although the A/D card has two analog input channels, the data throughput requirements of operating both channels at 100 percent duty cycle in parallel exceed the sustained data transfer rate of the PCIe data connection (8 lanes) and board drivers. To enable data capture on two channels at full acquisition rates, two identical A/D cards (X5-400M, Innovative Integration) were used simultaneously, as supported by the independence of PCIe architecture. Digital galvanometers (Cambridge Technology) were driven by a 16 bit D/A board (National Instruments). A custom user interface and data acquisition software was developed in C++ to coordinate instrument control and enable user interaction.

Improved performance for the retina and anterior angle imaging configurations was obtained by modifying a commercially available 350MHz InGaAs (Thorlabs) dual balanced detector to increase the transimpedance gain by 2X and reduce the bandwidth to ~200MHz. A stock 350MHz dual balanced detector (Thorlabs) was used for the long imaging range anterior segment imaging with the digital scope set to sample at 1 GSPS for data acquisition. Wavelength dependence in the 50:50 fiber coupler before the detectors causes an imbalance in the reference arm signal as the laser is swept, resulting in a significant background in the dual balanced detection. The low frequency background occupied 2–4 bits of the A/D range, leaving only 10–12 of the 14 bits to digitize the fringe. When the digital storage scope was used to record the signal at 1 GSPS, only 8 bit digitization was possible and a high pass filter (Mini-circuits 50MHz high pass filter) was used to remove the background. This filter also blocked interferometric signals near the zero delay, over the first 1mm imaging range.

3. System performance specifications and characterization

Table 1 presents an overview of the four different OCT imaging configurations. Configuration (A) images at a speed of 100kHz using the optically synthesized A/D clock. The sensitivity is 97dB with 5.3μm axial resolution and 2.9mm imaging range in tissue. Configuration (B) images at a speed of 100kHz using a digital storage scope set to sample at 1 GSPS. The sensitivity is 94dB with 6.0μm axial resolution and 7.5mm imaging range in tissue. Configuration (C) images at a speed of 200kHz using a data acquisition card running at fixed sampling rate of 400 MSPS. The sensitivity is 95dB with 5.3μm axial resolution and 3.8mm imaging range in tissue. Configuration (D) images at a speed of 400kHz using two imaging spots, two interferometers, and two 400 MSPS data acquisition cards. The sensitivity is 94dB with 5.3μm axial resolution and 3.8mm imaging range in tissue. The use of a 70:30 fiber coupler for configuration (D) improves sensitivity in the buffered configuration compared to the 50:50 fiber coupler in configuration (C), as explained in Section 2.1. The sensitivity roll-off measurements for the different configurations are shown in Fig. 3(A)–3(C), where the dual beam 400kHz configuration is similar to the 200kHz configuration. Figure 3(D) compares sensitivity roll-off for several spectral and swept source/Fourier domain OCT technologies [11, 32].

The sensitivity roll-off performance using the short cavity swept laser is significantly improved over previous spectral/Fourier domain and swept source/Fourier domain imaging results [Fig. 3(D)]. Figure 4 illustrates the practical importance of sensitivity roll-off performance by comparing images of the same retina at different depths using Fig. 4(A), a prototype 1050nm spectral/Fourier domain, Fig. 4(B), a prototype 850nm spectral/Fourier domain, and Fig. 4(C), the swept source system described in this paper. The zero delay is at the top in all images. Standard commercial ophthalmic OCT imaging systems have 6dB of sensitivity rolloff at ~1.3mm with ~5μm axial resolution in tissue using a spectrometer camera with 2048 pixels [33]. The 1050nm spectral/Fourier domain instrument has ~7μm axial resolution in tissue with ~97dB sensitivity and images at 47kHz axial scan rate using a spectrometer camera with 1024 pixels (Sensors Unlimited SU1024LDH-1.7RT). The 850nm spectral/Fourier domain instrument has ~3μm axial resolution in tissue with ~93dB sensitivity and images at 92kHz axial scan rate using 3072 spectrometer camera pixels (Basler Sprint spL4096-140k). The CMOS camera enables 3–4× faster line rates and improved axial resolution of ~3μm while maintaining sensitivity roll-off performance similar to commercial systems because of the ability to use 3072 camera pixels. Both spectral/Fourier domain systems have significant sensitivity loss with increasing depth. The sensitivity roll-off is so severe, that the 850nm spectral system is essentially unusable in the lower half of the imaging range. For the swept source system, the image at the deepest depth has a signal which is nearly indistinguishable from the image near the zero delay. The superior roll-off performance and long imaging range of the swept source OCT using a short cavity laser promises to improve performance in clinical ophthalmology, where long imaging ranges are important due to patient axial eye movement.

4. Ophthalmic imaging results

The prototype OCT instruments were used to image the human retina and anterior segment. Study protocols were approved by the institutional review board of the Massachusetts Institute of Technology. Written informed consent was obtained prior to the study. Retinal and anterior segment imaging was performed with an incident average power of 1.8mW-1.9mW, consistent with American National Standards Institute (ANSI) [34] standards and with exposure levels used in other research OCT ophthalmic instruments at 1050nm.

4.1. Retinal imaging at 100,000 and 200,000 axial scans per second

OCT cross-sectional images of the macula and optic disc consisting of 500 and 2000 axial scans were acquired using configurations A and C at 100kHz and 200kHz axial scan rates, respectively. As seen in Fig. 5, the images acquired at 100kHz show good signal to noise and deep penetration into the optic nerve head and choroid. The 5.3μm axial resolution enables delineation of the photoreceptor layers. The dynamic range in the 100kHz axial scan rate images as shown from left to right is 51.9dB (500 pixel macula), 54.8dB (500 pixel ONH), 54.1dB (2000 pixel macula), and 56.3dB (2000 pixel ONH). The image dynamic range was calculated as $20log_{10}$(peak image intensity / standard deviation of noise floor at 3/4 imaging depth range). The 200kHz axial scan rate images show noticeably reduced signal strength and reduced image penetration, although the signal is still quite high. The slight loss in axial resolution due to the overlap of the spectrum in the buffered laser configuration does not significantly compromise the image quality. The dynamic range in the 200kHz images as shown from left to right is 49.3dB (500 pixel macula), 48.0dB (500 pixel ONH), 50.1dB (2000 pixel macula), and 48.3dB (2000 pixel ONH).

All images were processed with zero padding to 4096 data points before Fourier transform and numerical dispersion compensation was applied. A fixed pattern noise appears to originate from the swept laser source and results in multiple horizontal lines across the image. Subtracting a background image (obtained by directing the galvos away from the sample to a position outside the optical aperture) from the sample image reduced fixed pattern noise and increased image dynamic range. Image background subtraction was performed for all images shown.

Averaging of rapidly repeated OCT cross sectional scans can increase signal to noise and decrease speckle. Figure 6 shows images consisting of an average of 10 registered frames using ImageJ (National Institutes of Health). In the macula image shown in Fig. 6(A), the back of the choroid can be seen and the cone outer segment tips can be clearly located in the photoreceptor layers when looking at the zoomed image (black arrow). A zoom of the optic disk shown in Fig. 6(B) demonstrates the high axial resolution by showing delineation of the inner photoreceptor layers (black arrow) and clear separation of layers in the area of the choroid, Bruch's membrane and RPE (white arrow).

The ultrahigh imaging speeds of the 1050nm swept source system enable the acquisition of dense 3D raster scanned volumes. Figure 7 shows 3D-OCT data of the optic disc at 100kHz axial scan rate consisting of 500×500 axial scans over 6mmx6mm acquired in 2.6 seconds and 200kHz consisting of 700×700 axial scans over 6mmx6mm also acquired in 2.6 seconds. Motion in the transverse direction is minimal, as shown in the OCT fundus images Figs. 7(A) and 7(D). Both 100kHz and 200kHz axial scan rate 3D-OCT data sets have similar acquisition times and have similar axial motion profiles, as can be seen in the 3D volumetric renderings [Figs. 7(C) and 7(F)]. Compared with the 200×200 uniformly sampled volumetric data over 6mm×6mm that can be obtained with the Zeiss Cirrus (and other commercial instruments) with 30μm/pixel sampling, the high density 500×500 and 700×700 axial scan data sets enable visualization of smaller features as allowed by the higher sampling densities of 12μm/pixel and 9μm/pixel, respectively, which should improve ability to register and compare data volumes for tracking small retinal changes over time.

Acquisition at 200kHz axial scan rate enables the collection of wide field of view, large data sets. Figure 8(A) shows a 1100×1100 axial scan image over 12mmx12mm acquired in ~6.3 seconds. A 64 bit operating system and acquisition software was required to accommodate the ~6 Gigabytes of raw data that results from this large acquisition. This data set provides comprehensive visualization of the optic nerve head and macular regions. Nerve fiber bundle orientations can be clearly seen in the OCT fundus image in addition to patterns from

large vessels within the choroid. The OCT fundus image in Fig. 8(A) compares to the standard fundus camera image in Fig. 8(B) of the same eye and illustrates the wide retinal coverage. Figures 8(C) and 8(D) show cross sectional images extracted from the 3D volume. The cross section through the optic nerve head (C), macula (D), and an average of 5 neighboring cross sectional scans (E) show good signal strength and deep image penetration. Averaging neighboring cross sectional images improves signal to noise and reduces speckle. However, increasing the number of averaged neighboring cross sections results in image blurring and loss of resolution because averaging is performed over an increasingly large lateral area. A beam diameter of 1.4mm on the eye was used to enable the wide field imaging. Figure 8(F) shows a 3D volumetric rendering of the large area 3D-OCT data.

Adaptive optics OCT (AO-OCT) enables the visualization of cone photoreceptors by correcting for ocular aberrations when imaging with a large beam diameter entering the eye to achieve fine lateral resolution of ~2–5μm. A complementary technology, ultrahigh speed OCT, has been shown to aid in the visualization of small features, such as cone photoreceptors and small retinal capillaries, by reducing image distortion and blurring caused by eye motion [11, 33].

For imaging of cone photoreceptors at an ultrahigh speed of 200kHz axial scan rate, the retinal patient interface optics were changed to obtain a larger beam diameter of 3.3mm entering the eye. Without adaptive optics, larger beam diameters produce smaller spots on the retina, but only up to limits where uncorrected ocular abberations dominate. Figure 9 demonstrates small volume, high sampling density retinal imaging, showing the cone mosaic imaged at 200kHz axial scan rate. Multiple volumes of 600×600 axial scans over a 700μmx700μm region were acquired in 2 seconds each. The volumes span a region between the fovea and optic nerve head with slight overlap. Image processing was performed to identify the photoreceptor layer boundaries. *En face* images were then formed by depth summing over the photoreceptors in linearly scaled data, which has been shown to yield higher contrast images of cone photoreceptors than log scaling [35]. Postprocessing registration was performed on the *en face* images to remove small eye movements and artifacts resulting from a slight mismatch between axial acquisition rate and galvo trajectory generation. The resulting *en face* images were assembled together to form a large composite image, similar to what has been performed with AO-OCT [36]. Individual cones can be identified in images acquired in the same area, suggesting that in certain regions of the retina it is possible to track individual cone photoreceptors longitudinally over time. Referring to the zoomed in images in Fig. 9(1Z)–9(6Z), the size and spacing of the cones decreases moving from the disc to the fovea, showing arrangement and patterns consistent with histology [37,38]. Near the fovea, individual cones can no longer be distinguished, Figs. 9(7Z) and 9(7ZF). Imaging of individual cone photoreceptors closer to the fovea, or in eyes with significant aberration, as is often the case with older patients, would require adaptive optics OCT technology. The ability to identify individual cone photoreceptors and other small features in different data sets taken at different times promises to shorten the time periods over which small changes to the retinal structure can be detected, as well as improve the ability to detect and monitor focal disease.

High speed imaging also enables rapid repeated volume imaging (4D-OCT). 4D-OCT has been shown to improve visualization of the small retinal capillaries through motion contrast [11], as an alternative to speckle variance and Doppler OCT. 4D-OCT is also important for capturing dynamic processes for functional imaging experiments, as well as for improving signal to noise through volumetric data averaging of structural OCT data.

4.2. Anterior segment imaging at 100,000 axial scans per second

OCT imaging of the anterior segment enables visualization of the cornea, tear film, lens, iris, and outflow features, such as Schlemm's canal and the trabecular meshwork. Many commercial OCT retinal imaging instruments offer an adapter to enable scanning the anterior segment. Ultrahigh speed prototype anterior segment OCT imaging systems have been demonstrated with 6.9–15.4μm axial resolution at 850nm using spectral / Fourier domain detection at up to 135kHz [39] and with 9–25μm axial resolution at 1310nm using swept source / Fourier domain detection at 200kHz [21]. The commercially available Zeiss Visante achieves 18μm axial resolution at 1310nm with 16mmx6mm scan range using time domain detection.

Figures 10(A)–10(D) show images obtained with the 1050nm swept source/Fourier domain instrument using configuration A with a 50mm focal length scan lens placed after the galvo scanners [see Fig. 1(D)]. A 3D volumetric rendering of the anterior angle is shown in Fig. 10(A). An average of two neighboring cross sectional images is shown in Fig. 10(B). The polarization artifact associated with the trabecular meshwork (TM) and Schlemm's canal (SC) itself can be seen in the full size, Fig. 10(B), and zoomed in image, Fig. 10(C). An *en face* OCT image consisting of 2 averaged *en face* plane extractions is shown in Fig. 10(D). The *en face* plane is at an elevation indicated by the dashed line in Fig. 10(C), which intersects Schlemm's canal. Deep image penetration enables visualization of the iris and anterior angle through the sclera. The 1050nm imaging system achieves considerably higher axial resolution of 5.3μm when compared to 1310nm anterior eye imaging. The 1050nm imaging also demonstrates increased penetration when compared to 850nm imaging. Imaging at 1050nm may provide attractive imaging characteristics of high axial resolution and deep penetration for anterior imaging.

Figure 10(E) shows a cross sectional image from the extended imaging range configuration B that uses a digital storage scope sampling at 1 GSPS. Limited memory of the digital storage scope enables only a single cross sectional image at this sampling density. The image consists of 4500 axial scans over 17mm and shows the cornea, iris, and anterior surface of the lens in a single image. The long imaging range is enabled by the long coherence length of the short cavity laser and high 1 GSPS rate of the oscilloscope acquisition. Each fringe is digitized by 4700 sample points resulting in 2350 pixels spanning the 7.5mm imaging range in tissue. A longer focal length scan lens (80mm) was used to increase the Raleigh range (depth of focus) of this configuration to match the long imaging range, however, the larger resulting spot compromises lateral resolution. The ability to image over long imaging range and with high axial and lateral resolution promises to improve diagnostics and visualization of the anterior eye.

4.3. Dual spot imaging at 400,000 axial scans per second

Ultrahigh speed ophthalmic OCT imaging has been performed using high speed CMOS camera technology for spectral/Fourier domain detection and FDML swept wavelength light sources for swept source/Fourier domain detection. Higher imaging speeds enable the collection of greater density data sets within practical acquisition times limited by patient eye motion and blinking. However, as OCT imaging speeds increase, the associated decrease in sensitivity results in an upper bound on practical imaging speeds. Multi-spot scanning with parallel acquisition channels may offer an alternative path to achieving ultrahigh imaging speeds in the ophthalmic clinic and for research applications. Multiple spot OCT has been used in commercial OCT instruments for imaging external tissues (Michelson Diagnostics), for high sensitivity ophthalmic Doppler OCT [40], and to achieve record imaging speed in research OCT applications in a microscope configuration [19].

We developed a dual spot / dual interferometer ophthalmic imaging instrument that acquires data at 400,000 axial scans per second. Two spots were projected on the retina, as shown in Fig. 11(A). The power in each beam was 950μ W, such that the combined total power on the eye was 1.9mW. The spots were separated by ~4.5mm on the retina in the y direction, such that a raster scan with x priority acquires two volumes simultaneously. Renderings of the two volumes are presented in Fig. 11(B) and show identical axial eye motion profiles due to the simultaneous acquisition. Fig. 11(C) shows the OCT fundus image of the combined data sets. With 7% overlap between the images, the total acquisition time was 2.9 seconds. Figure 11(D) shows a cross section through the optic disc acquired from the first interferometer channel and Fig. 11(E) shows a cross section through the fovea acquired from the second interferometer channel. In the future, pending analysis and IRB approval, it should be possible to use 1.9mW in each channel for improved sensitivity. Compared to the 12mmx12mm wide field of view, large data set presented in Section 4.1 acquired with a ~6.3 second acquisition, the dual spot imaging system reduces the acquisition time by approximately a factor of two.

5. Conclusions

We demonstrated ophthalmic OCT imaging at speeds of 100,000–400,000 axial scans per second with a 1050nm swept source/Fourier domain prototype instrument using a short cavity laser. Four imaging configurations were characterized and demonstrated for retinal and anterior segment imaging. An optically clocked A/D configuration (A) images at 100kHz axial scan rate and samples the fringe at equal k intervals. Although dispersion compensation is still required, this approach significantly decreases processing time by eliminating the fringe recalibration step. Dense volumetric acquisitions of the fovea, disc, and anterior angle show strong signal and good resolution. Configuration (B) demonstrates a long imaging range of 7.5mm in tissue by using a digital storage scope set to acquire at 1 GSPS sampling rate and numerical fringe k calibration. With the long imaging range, the entire anterior segment from the cornea, though the iris, to the anterior of the lens can be directly imaged without the need for complex conjugate full range imaging techniques, which typically exhibit artifacts due to incomplete mirror image suppression. Configuration (C) uses sweep buffering and multiplexing to double the sweep rate to 200kHz. At this high imaging speed, wide field 12mmx12mm (1100×1100 axial scan) 3D-OCT data sets spanning both the macula and optic disc can be acquired for comprehensive visualization of the maculo-papilla region of the retina. Small field, high sampling density imaging can show fine retinal features, such as individual photoreceptors. The ultra-high imaging speeds are important for reducing image distortion and blurring, as well as for acquiring dense axial scan spacing needed to visualize small features. Configuration (D) uses two imaging spots in the eye and two parallel interferometers to achieve 400kHz axial scan rate imaging speeds. This is almost two times faster than previously demonstrated swept source 1050nm retinal imaging and twenty times faster than current commercial OCT instruments.

All configurations show long imaging range with a low sensitivity roll-off, which can be achieved with swept source / Fourier domain OCT using narrow linewidth swept lasers. Compared with 850nm spectral/Fourier domain imaging using CMOS cameras at comparable speeds [11], signal strength and image penetration is higher for the 1050nm swept source system because of the higher instrument sensitivity, improved sensitivity roll-off performance, and reduced scattering at 1050nm. Axial resolution using the 1050nm swept source/Fourier domain system is 5.3μm in the retina at 100,000–400,000 axial scan rate, which is better than the 8–9μm axial resolution in the 850nm spectral system at 250,000–312,500 axial scan rate [11].

The commercially available short cavity swept laser (Axsun Technologies) used in this investigation has a narrow instantaneous linewidth and broad sweep bandwidth, enabling a long imaging range and fine axial resolution. The swept source OCT system using a short cavity swept laser achieves 5.3μm axial resolution in tissue, which is a finer resolution than previously reported swept source imaging results with 8.0μm axial resolution using an FDML laser at 250,000 axial scans per second [20]. FDML laser sweep bandwidths and image resolutions are limited by dispersion in the intracavity optical fiber delay at 1050nm wavelengths, suggesting that short cavity swept lasers may offer better performance for these wavelengths. Compared with previous swept lasers which had cavity round trip lengths approaching fractions of a meter and operated at axial scan rates of ~20–30kHz [12, 28], a few centimeter short cavity swept laser can achieve higher sweep speeds and narrower instantaneous line widths. The sweep speed of the laser is governed by the time needed to build up lasing from amplified spontaneous emission noise to saturate the gain medium as the laser is dynamically tuned, hence the short round trip times enable a fundamental increase in sweep speed [17]. Currently, multiple companies are developing compact, short cavity swept lasers for the OCT market.

Swept source/Fourier domain detection has advantages compared with spectral/Fourier domain OCT, including reduced fringe washout, lower sensitivity roll off, longer imaging range, higher detection efficiencies (because there are no spectrometer grating losses) and ability to performed dual balanced detection, enabling reduced A/D bit depth. At the same time, swept source OCT is very sensitive to excess intensity noise in the swept laser and careful attention to balanced detection is required. In addition, swept source OCT is sensitive to parasitic re-flections since combinations of reflections at any point in the optical system can interfere to produce beat frequencies, resulting in pattern noise. However, swept source OCT offers several engineering advantages because polarization diversity or polarization sensitive detection can be implemented more easily than in spectrometer based spectral OCT. Finally swept source OCT can be made more compact than spectral OCT because bulky spectrometers are not required.

The improvements in imaging speed and imaging depth range achieved by swept source OCT are important advantages for ophthalmic imaging. The ability to rapidly acquire 3D-OCT data over a wide field of view promises to simplify ophthalmic examination protocols. The ability to zoom and image fine structures with high speed and high density can provide detailed information on focal pathologies. The large imaging range and improved image penetration at 1050nm wavelengths promises to improve performance for ophthalmic instrumentation which images both the retina and anterior eye. These advantages suggest that swept source OCT at 1050nm wavelengths will play an important role in future ophthalmic instrumentation.

Acknowledgments

This research is sponsored in part by the National Institutes of Health 5R01-EY011289-23, 5R01-EY013178-10, 2R01-EY013516-07, 1R01-EY019029-02, Air Force Office of Scientific Research contract FA9550-07-1-0014 and Medical Free Electron Laser Program contract FA9550-07-1-0101. We thank Tsung-Han Tsai, Chao Zhou, Jonathan J. Liu, Hsiang-Chieh Lee and Martin F. Kraus for valuable discussions and assistance related to the paper.

References and links

1. Huang D, Swanson EA, Lin CP, Schuman JS, Stinson WG, Chang W, Hee MR, Flotte T, Gregory K, Puliafito CA, Fujimoto JG. Optical coherence tomography. Science. 1991; 254(5035):1178–1181. [PubMed: 1957169]
2. Schuman, JS.; Puliafito, CA.; Fujimoto, JG. Optical Coherence Tomography of Ocular Diseases. Slack, Inc; New Jersey, USA: 2004.

3. Chinn SR, Swanson EA, Fujimoto JG. Optical coherence tomography using a frequency-tunable optical source. Opt Lett. 1997; 22(5):340–342. [PubMed: 18183195]
4. de Boer JF, Cense B, Park BH, Pierce MC, Tearney GJ, Bouma BE. Improved signal-to-noise ratio in spectral-domain compared with time-domain optical coherence tomography. Opt Lett. 2003; 28(21):2067–2069. [PubMed: 14587817]
5. Leitgeb R, Hitzenberger C, Fercher A. Performance of fourier domain vs. time domain optical coherence tomography. Opt Express. 2003; 11(8):889–894. [PubMed: 19461802]
6. Choma M, Sarunic M, Yang C, Izatt J. Sensitivity advantage of swept source and Fourier domain optical coherence tomography. Opt Express. 2003; 11(18):2183–2189. [PubMed: 19466106]
7. Wojtkowski M, Leitgeb R, Kowalczyk A, Bajraszewski T, Fercher AF. In vivo human retinal imaging by Fourier domain optical coherence tomography. J Biomed Opt. 2002; 7(3):457–463. [PubMed: 12175297]
8. Cense B, Nassif N, Chen T, Pierce M, Yun SH, Park B, Bouma B, Tearney G, de Boer J. Ultrahigh-resolution high-speed retinal imaging using spectral-domain optical coherence tomography. Opt Express. 2004; 12(11):2435–2447. [PubMed: 19475080]
9. Leitgeb R, Drexler W, Unterhuber A, Hermann B, Bajraszewski T, Le T, Stingl A, Fercher A. Ultrahigh resolution Fourier domain optical coherence tomography. Opt Express. 2004; 12(10): 2156–2165. [PubMed: 19475051]
10. Wojtkowski M, Srinivasan V, Ko T, Fujimoto J, Kowalczyk A, Duker J. Ultrahigh-resolution, high-speed, Fourier domain optical coherence tomography and methods for dispersion compensation. Opt Express. 2004; 12(11):2404–2422. [PubMed: 19475077]
11. Potsaid B, Gorczynska I, Srinivasan VJ, Chen Y, Jiang J, Cable A, Fujimoto JG. Ultrahigh speed Spectral/Fourier domain OCT ophthalmic imaging at 70,000 to 312,500 axial scans per second. Opt Express. 2008; 16(19):15149–15169. [PubMed: 18795054]
12. Lee EC, de Boer JF, Mujat M, Lim H, Yun SH. In vivo optical frequency domain imaging of human retina and choroid. Opt Express. 2006; 14(10):4403–4411. [PubMed: 19516592]
13. Srinivasan VJ, Huber R, Gorczynska I, Fujimoto JG, Jiang JY, Reisen P, Cable AE. High-speed, high-resolution optical coherence tomography retinal imaging with a frequency-swept laser at 850 nm. Opt Lett. 2007; 32(4):361–363. [PubMed: 17356653]
14. de Bruin DM, Burnes D, Loewenstein J, Chen Y, Chang S, Chen T, Esmaili D, de Boer JF. In-vivo three-dimensional imaging of neovascular age related macular degeneration using optical frequency domain imaging at 1050 nm. Invest Ophthalmol Vis Sci. 2008; 07:1553.
15. Lim H, de Boer JF, Park BH, Lee EC, Yelin R, Yun SH. Optical frequency domain imaging with a rapidly swept laser in the 815–870 nm range. Opt Express. 2006; 14(13):5937–5944. [PubMed: 19516763]
16. Lim H, Mujat M, Kerbage C, Lee EC, Chen Y, Chen TC, de Boer JF. High-speed imaging of human retina in vivo with swept-source optical coherence tomography. Opt Express. 2006; 14(26): 12902–12908. [PubMed: 19532183]
17. Huber R, Wojtkowski M, Taira K, Fujimoto J, Hsu K. Amplified, frequency swept lasers for frequency domain reflectometry and OCT imaging: design and scaling principles. Opt Express. 2005; 13(9):3513–3528. [PubMed: 19495256]
18. Huber R, Wojtkowski M, Fujimoto JG. Fourier Domain Mode Locking (FDML): A new laser operating regime and applications for optical coherence tomography. Opt Express. 2006; 14(8): 3225–3237. [PubMed: 19516464]
19. Wieser W, Biedermann BR, Klein T, Eigenwillig CM, Huber R. Multi-Megahertz OCT: High quality 3D imaging at 20 million A-scans and 4.5 GVoxels per second. Opt Express. 2010; 18(14): 14685–14704. [PubMed: 20639955]
20. Srinivasan VJ, Adler DC, Chen Y, Gorczynska I, Huber R, Duker J, Schuman JS, Fujimoto JG. Ultrahigh-speed Optical Coherence Tomography for Three-Dimensional and En Face Imaging of the Retina and Optic Nerve Head. Invest Ophthalmol Vis Sci. 2008; 08:2127.
21. Gora M, Karnowski K, Szkulmowski M, Kaluzny BJ, Huber R, Kowalczyk A, Wojtkowski M. Ultra high-speed swept source OCT imaging of the anterior segment of human eye at 200 kHz with adjustable imaging range. Opt Express. 2009; 17(17):14880–14894. [PubMed: 19687967]

22. Unterhuber A, Povazay B, Hermann B, Sattmann H, Chavez-Pirson A, Drexler W. In vivo retinal optical coherence tomography at 1040 nm - enhanced penetration into the choroid. Opt Express. 2005; 13(9):3252–3258. [PubMed: 19495226]
23. Yasuno Y, Hong Y, Makita S, Yamanari M, Akiba M, Miura M, Yatagai T. In vivo high-contrast imaging of deep posterior eye by 1-um swept source optical coherence tomography and scattering optical coherence angiography. Opt Express. 2007; 15(10):6121–6139. [PubMed: 19546917]
24. Hariri S, Moayed AA, Dracopoulos A, Hyun C, Boyd S, Bizheva K. Limiting factors to the OCT axial resolution for in-vivo imaging of human and rodent retina in the 1060nm wavelength range. Opt Express. 2009; 17(26):24304–24316. [PubMed: 20052141]
25. Chen Y, Burnes DL, de Bruin M, Mujat M, de Boer JF. Three-dimensional pointwise comparison of human retinal optical property at 845 and 1060 nm using optical frequency domain imaging. J Biomed Opt. 2009; 14(2):024016. [PubMed: 19405746]
26. Yasuno Y, Miura M, Kawana K, Makita S, Sato M, Okamoto F, Yamanari M, Iwasaki T, Yatagai T, Oshika T. Visualization of Sub-retinal Pigment Epithelium Morphologies of Exudative Macular Diseases by High-Penetration Optical Coherence Tomography. Invest Ophthalmol Vis Sci. 2009; 50(1):405–413. [PubMed: 18676629]
27. Esmaeelpour M, Povazay B, Hermann B, Hofer B, Kajic V, Kapoor K, Sheen N, North RV, Drexler W. Three-dimensional 1060nm OCT: Choroidal thickness maps in normals and improved posterior segment visualization in cataract patients. Invest Ophthalmol Vis Sci. 2010; 10:5196.
28. Yasuno Y, Madjarova VD, Makita S, Akiba M, Morosawa A, Chong C, Sakai T, Chan KP, Itoh M, Yatagai T. Three-dimensional and high-speed swept-source optical coherence tomography for in vivo investigation of human anterior eye segments. Opt Express. 2005; 13(26):10652–10664. [PubMed: 19503280]
29. Eigenwillig CM, Biedermann BR, Palte G, Huber R. K-space linear Fourier domain mode locked laser and applications for optical coherence tomography. Opt Express. 2008; 16(12):8916–8937. [PubMed: 18545605]
30. Adler DC, Chen Y, Huber R, Schmitt J, Connolly J, Fujimoto JG. Three-dimensional endomicroscopy using optical coherence tomography. Nat Photonics. 2007; 1(1):709–716.
31. Xi J, Huo L, Li J, Li X. Generic real-time uniform K-space sampling method for high-speed swept-Source optical coherence tomography. Opt Express. 2010; 18(9):9511–9517. [PubMed: 20588797]
32. Potsaid, B.; Liu, J.; Manjunath, V.; Gorczynska, I.; Srinivasan, VJ.; Jiang, J.; Barry, S.; Cable, A.; Duker, JS.; Fujimoto, JG. Ultrahigh-speed volumetric ophthalmic OCT imaging at 850nm and 1050nm. Vol. 7550. SPIE; 2010. p. 75501K
33. Považay B, Hofer B, Torti C, Hermann B, Tumlinson AR, Esmaeelpour M, Egan CA, Bird AC, Drexler W. Impact of enhanced resolution, speed and penetration on three-dimensional retinal optical coherence tomography. Opt Express. 2009; 17(5):4134–4150. [PubMed: 19259251]
34. American National Standards Institute. American National Standard for Safe Use of Lasers, ANSI Z136.1. 2000.
35. Zhang Y, Cense B, Rha J, Jonnal RS, Gao W, Zawadzki RJ, Werner JS, Jones S, Olivier S, Miller DT. High-speed volumetric imaging of cone photoreceptors with adaptive optics spectral-domain optical coherence tomography. Opt Express. 2006; 14(10):4380–4394. [PubMed: 19096730]
36. Zawadzki RJ, Choi SS, Fuller AR, Evans JW, Hamann B, Werner JS. Cellular resolution volumetric in vivo retinal imaging with adaptive optics–optical coherence tomography. Opt Express. 2009; 17(5):4084–4094. [PubMed: 19259248]
37. Hirsch J, Curcio CA. The spatial resolution capacity of human foveal retina. Vis Res. 1989; 29:1095–1101. [PubMed: 2617858]
38. Curcio CA, Sloan KR, Kalina RE, Hendrickson AE. Human photoreceptor topography. J Comp Neurol. 1990; 292:497–523. [PubMed: 2324310]
39. Grulkowski I, Gora M, Szkulmowski M, Gorczynska I, Szlag D, Marcos S, Kowalczyk A, Wojtkowski M. Anterior segment imaging with Spectral OCT system using a high-speed CMOS camera. Opt Express. 2009; 17(6):4842–4858. [PubMed: 19293916]
40. Makita, S.; Yamanari, M.; Miura, M.; Yasuno, Y. High-sensitive blood flow imaging of the retina and choroid by using double-beam optical coherence angiography. Vol. 7550. SPIE; 2010. p. 75500E

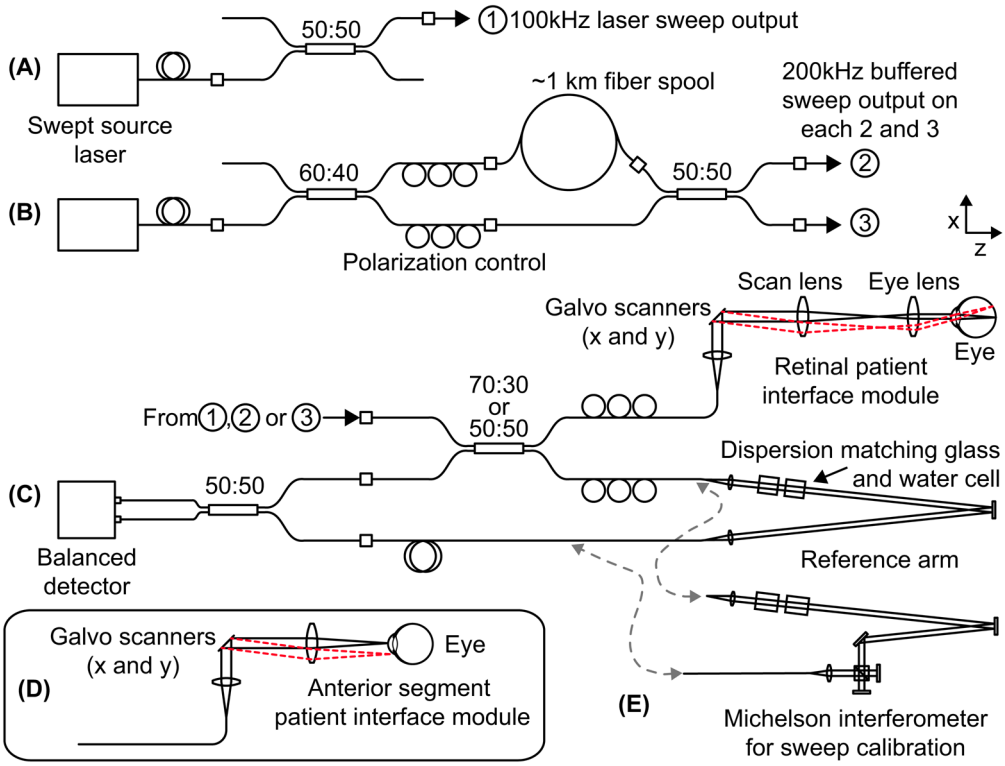

Fig. 1.

System layout. (A) Swept laser source for 100kHz OCT imaging. (B) Swept laser source for 200kHz and 400kHz OCT imaging. (C) System configuration for retinal imaging. (D) Patient interface for anterior segment imaging. (E) System configuration for sweep calibration.

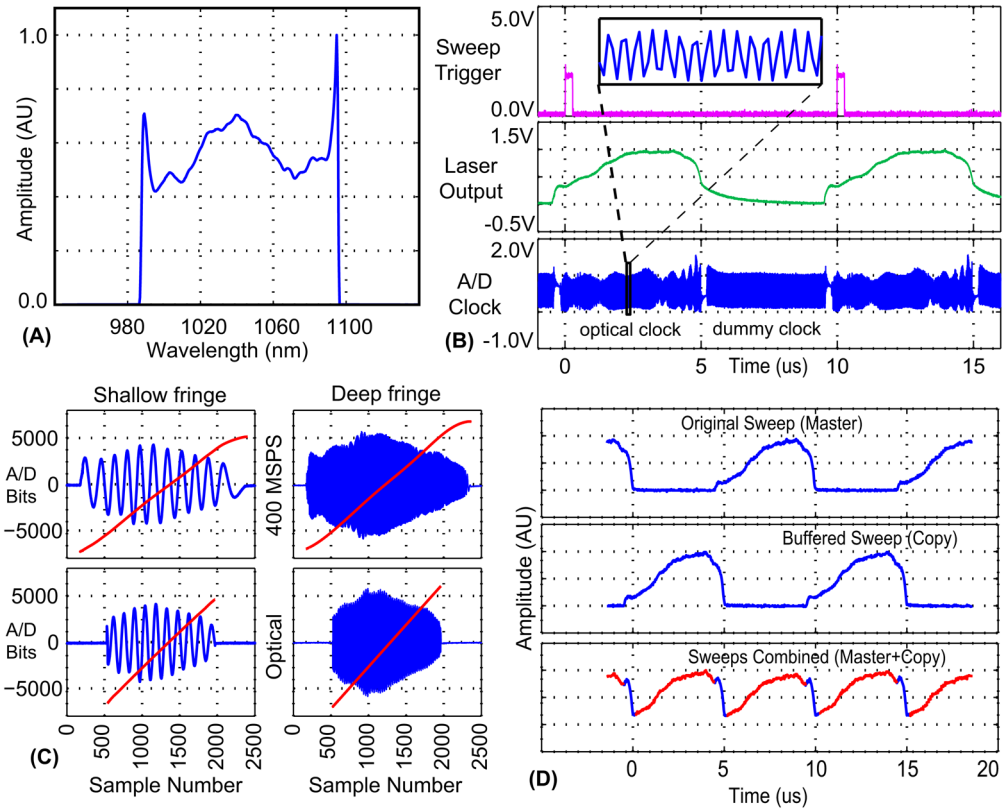

Fig. 2.

Short cavity light source. (A) Spectrum measured with OSA. (B) Sweep trigger signal, laser output, and A/D clock signal from the swept laser source. (C) OCT fringe data acquired at fixed 400 MSPS clock rate (top) and optically derived, variable frequency A/D clock (bottom) of a shallow fringe (left) and deep fringe (right). The red line indicates the phase of the fringe. (D) Laser sweeps from buffered configuration showing master sweep (top), copy sweep (middle), and combined master and copy sweeps (bottom). The usable portion of the sweep, considering sweep overlap, is indicated in red.

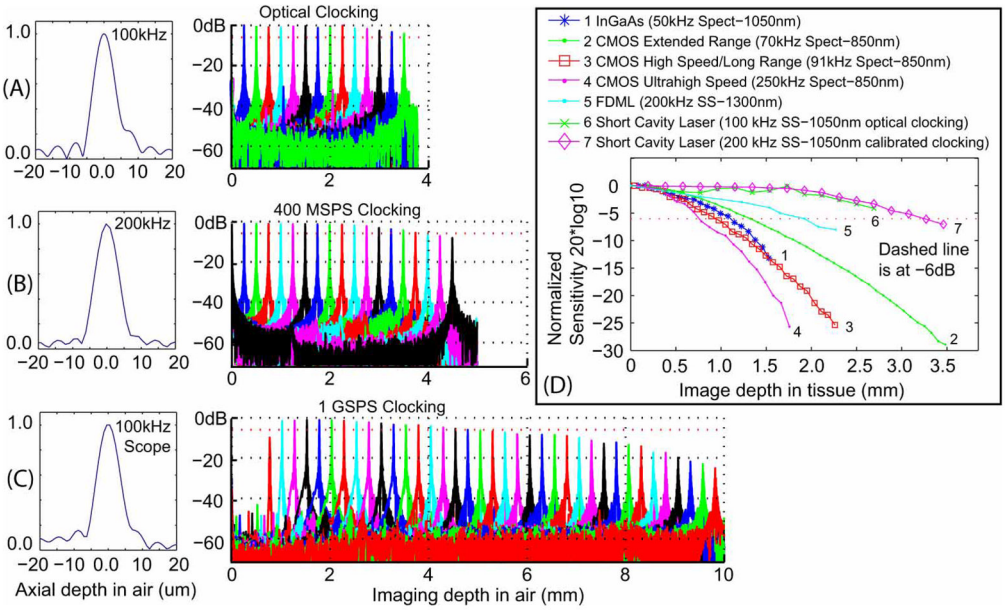

Fig. 3.

Point Spread Function (PSF) and sensitivity roll-off plot comparisons. (A) 100kHz axial scan rate configuration with optical A/D clocking. (B) 200kHz and 400kHz axial scan rate configurations with fixed 400 MSPS internal A/D clocking. (C) 100kHz axial scan rate configuration with digital storage scope acquisition at 1 GSPS. (D) Comparison of sensitivity roll-off performance for different OCT technologies.

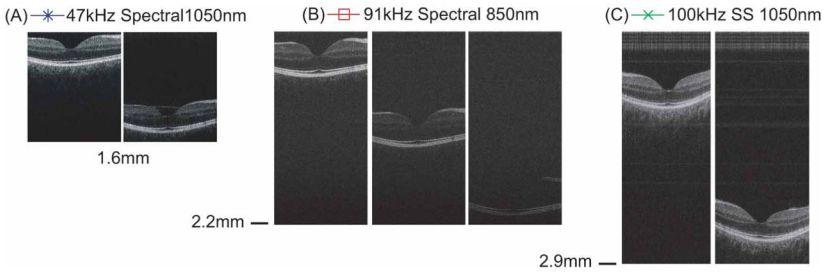

Fig. 4.

Depth range and sensitivity roll-off comparison of different OCT technologies demonstrated with retinal imaging of the same eye. Plots of the sensitivity roll-off performance for the different configurations shown are displayed in Fig. 3D, as indicated by the marker symbols.

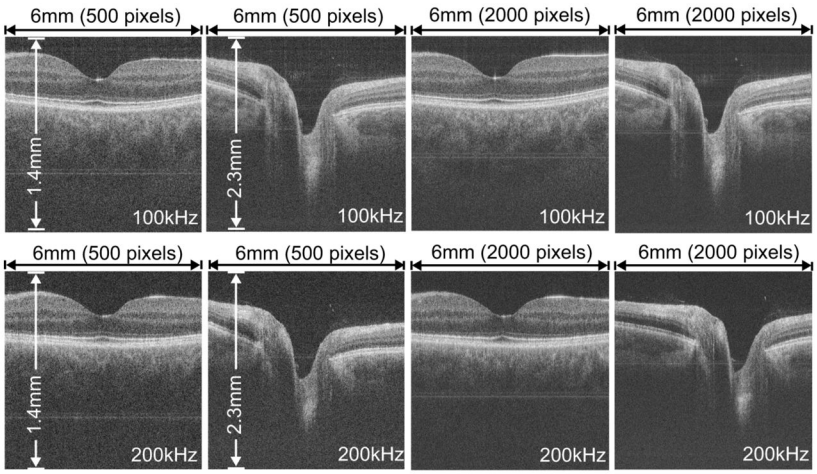

Fig. 5.

Comparison of cross sectional OCT retinal images acquired at 100kHz and 200kHz axial scan rate of the macula and optic disc. Images are cropped in depth to span 1.4mm for the macula and 2.3mm for the disc.

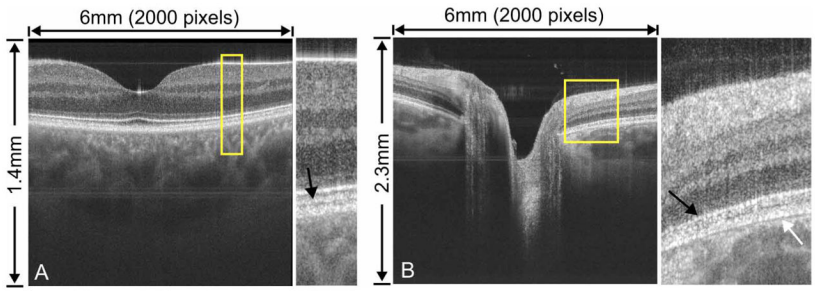

Fig. 6.

Images of the (A) macula and (B) optic disc consisting of an average of 10 rapidly repeated OCT cross sectional scans acquired at 100kHz axial scan rate. Images are cropped in depth to span 1.4mm for the macula and 2.3mm for the disc.

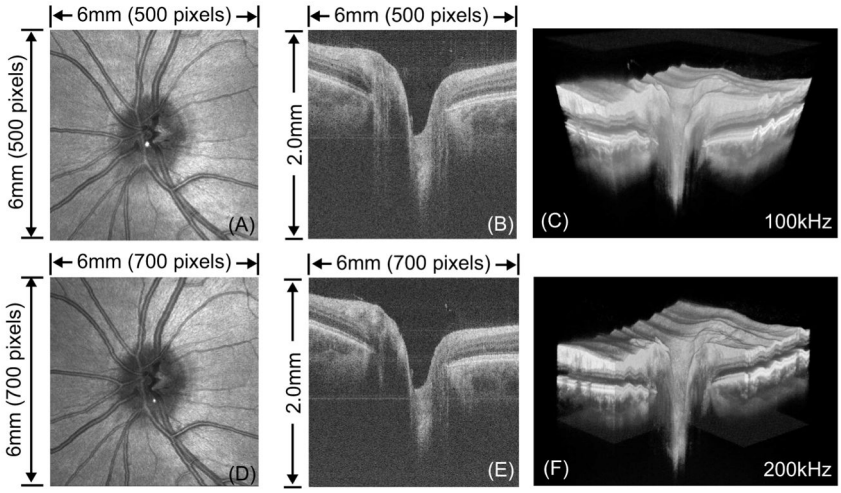

Fig. 7.

(A) OCT fundus image of 3D volume acquired at 100kHz with 500×500 axial scans over 6mmx6mm (2.6 sec). (B) 100kHz cross sectional image. (C) 3D volume rendering of 100kHz data (Media 1). (C) OCT fundus image of 3D volume acquired at 200kHz with 700×700 axial scans over 6mmx6mm (2.6 sec). (D) 200kHz cross sectional image. (E) 3D volume rendering of 200kHz data. Images are cropped in depth to span 2mm.

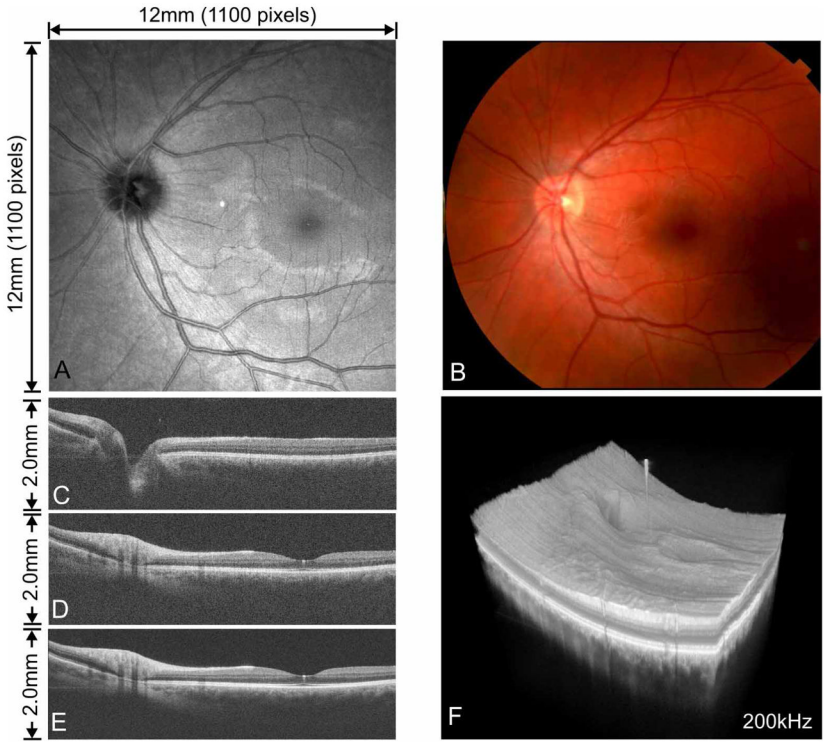

Fig. 8.

Large volume data sets acquired at 200kHz axial scan rate in 6.3 seconds consisting of 1100×1100 axial scans over 12mmx12mm. (A) OCT fundus image. (B) Fundus photo. (C) OCT cross sectional image through the disc. (D) OCT cross sectional image through the fovea. (E) Averaged image consisting of 5 adjacent OCT cross sectional images. (F) 3D rendering of volumetric OCT data. Images are cropped in depth to span 2.0mm.

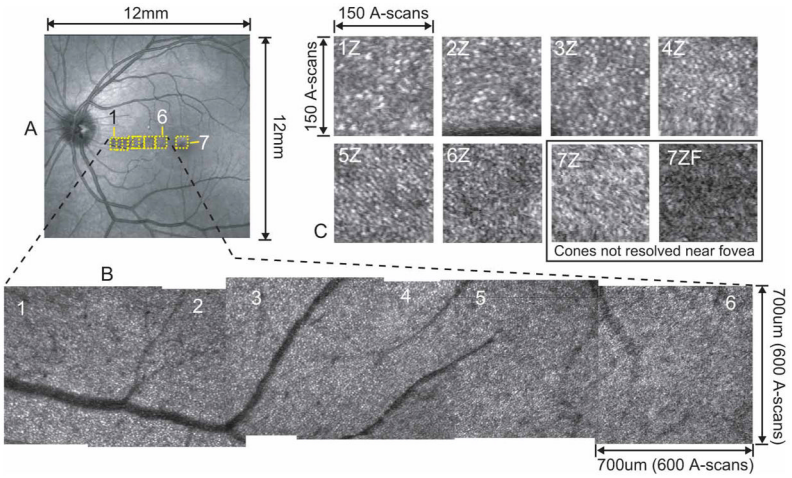

Fig. 9.

Cone imaging at 200kHz axial scan rate. (A) Large area OCT fundus view of retina showing boxes to indicate regions of cone imaging. (B) Cone photoreceptor mosaic formed by merging data from 6 volumes covering 700umx700um square patches consisting of 600×600 axial scans acquired in 2 seconds each. (C) Zoomed in images from volumes 1–7 are cropped to 150×150 axial scans and are shown in 1Z-7ZF. Individual cone photoreceptors can be clearly seen with decreasing size and spacing in the region progressing from the optic disc to the fovea in images 1Z-6Z. The small and closely spaced cones can not be resolved in 7Z, near the fovea, and 7ZF, located at the fovea center.

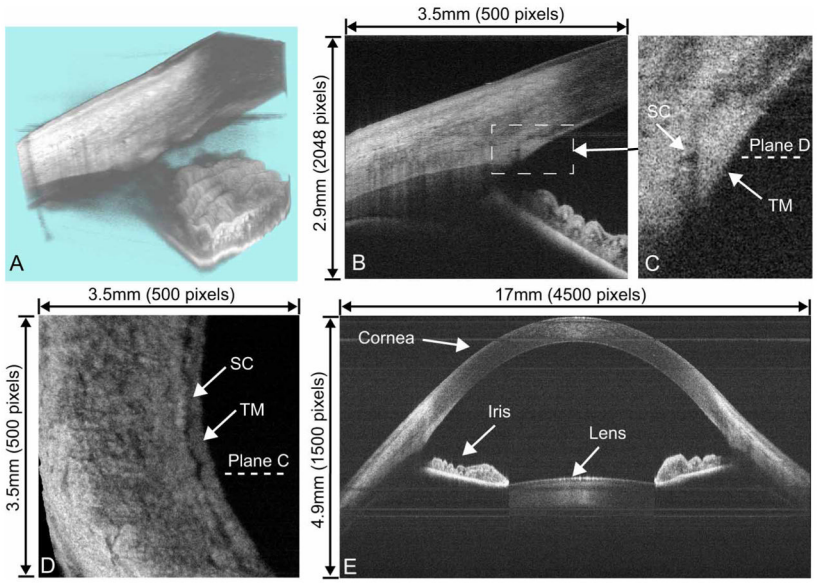

Fig. 10.

Anterior segment images acquired at 100kHz axial scan rate. (A) 3D OCT volume of the angle consisting of 500×500 axial scans over 3.5×3.5mm acquired in 2.6 seconds using optical clocking (Media 2). (B) Cross sectional image of the angle from (A) consisting of the average of two neighboring cross sectional scans. (C) Zoomed in region from (B) showing Schlemm's canal (SC) and the trabecular meshwork (TM). (D) OCT *en face* view extracted from (A) consisting of a depth averaged over 2 *en face* planes showing coronal section through structures related to outflow (Media 3). (E) OCT cross sectional image of the cornea, iris, and anterior lens acquired using 1 GSPS sampling with an oscilloscope showing high axial resolution imaging over a long imaging range. The image is cropped in depth to span 4.9mm.

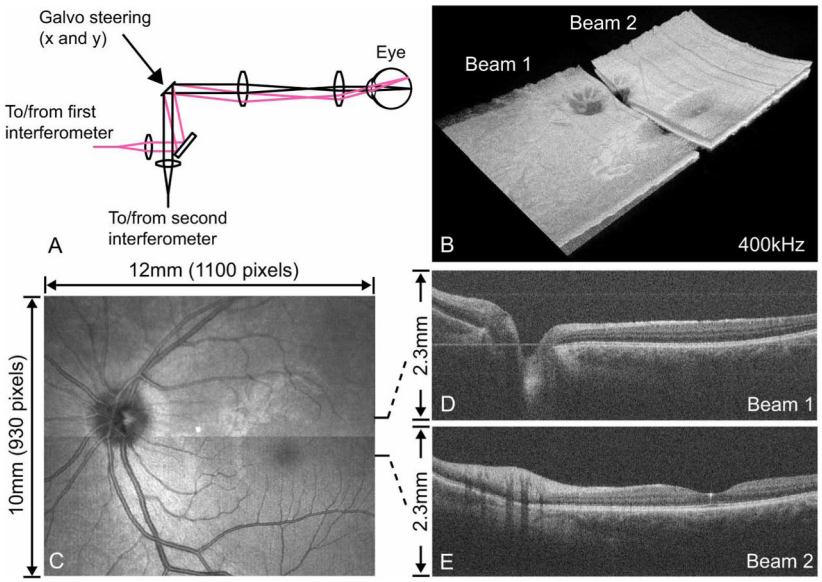

Fig. 11.

Dual OCT beam 400kHz axial scan rate imaging results. (A) Dual beam scanning system used in patient interface module. (B) 3D rendering showing the independent volumes that were acquired in parallel. (C) OCT fundus image generated from combining the two volumes acquired in parallel. (D) Example cross sectional OCT image acquired from first channel. (E) Example cross sectional OCT image acquired from second channel. Images are cropped in depth to span 2.3mm. The full data set was acquired in 2.9 seconds.

Table 1

System Design Configurations and Performance Measures

Design Configuration:	**A**	**B**	**C**	**D**
Axial Scan Rate	100,000	100,000	200,000	400,000
A/D Clocking Scheme	Optically Synthesized	Internal to Scope	Internal DAQ Oscillator	Internal DAQ Oscillator
A/D clocking rate	Variable	1 GSPS	400 MSPS	400 MSPS
Fringe Sample Points	1400	4700	1800	1800
Beam diameter on cornea for retinal imaging	1.4mm WF	-	1.4mm WF 3.3mm HR	1.4mm WF
NA for anterior segment imaging	0.035	0.024	-	-
Performance Measure:	A	B	C	D
Sensitivity (in air)	97dB	94dB	95dB	94dB
Imaging range in air	3.8mm	10mm	5.0mm	5.0mm
Imaging range in tissue*	2.9mm	7.5mm	3.8mm	3.8mm
6 dB roll-off depth in air	> full range	4.4mm	4.2mm	4.2mm
Axial resolution in air	7.0μm	8.0μm	7.1μm	7.1μm
Axial resolution in tissue*	5.3μm	6.0μm	5.3μm	5.3μm

WF: Wide field imaging configuration. HR: High resolution imaging configuration.

*Estimated from air measurement assuming n=1.33